J. Cent. South Univ. (2021) 28: 2647−2659
DOI: https://doi. org/10. 1007/s11771-021-4799-2

Springer

Influence of prolonged natural aging followed by artificial aging on tensile properties and compressive behavior of a thin-walled 6005 aluminum alloy tube

ZHANG Long(张龙)[1], LI Ke(李克)[2], HE Hong(何洪)[1]*, LI Luo-xing(李落星)[1]

1. State Key Laboratory of Advanced Design and Manufacturing for Vehicle Body, College of Mechanical and Vehicle Engineering, Hunan University, Changsha 410082, China;
2. AECC South Industry Co., Ltd., Zhuzhou 412002, China

Abstract: The effects of aging treatments on the tensile properties and compressive behavior of a thin-walled 6005 aluminum alloy tube were studied. Samples after three natural aging (NA) conditions were subsequently aged at 180 °C for 0.5−12.0 h artificial aging (AA). Tensile and compressive tests were performed after AA. The results show that for samples with the same NA, the longer the AA time is, the higher the strengths alloy owns, and at the same time the material shows a much lower elongation and faster process from plastic deformation to fracture. However, with NA prolonging, the alloy exhibits much better plastic deformation ability after AA, though its strength is decreased. The major cause of strength and plasticity variation induced by changing NA time is that the size of the main strengthening β'' precipitates is larger and the density is lower. This character is evaluated by the strain hardening exponent n. Compressive results show that the optimum energy absorption characteristics can be acquired at a moderate n ($14<n<17$). Large n ($n\geqslant 18$) results in the fracture of tube during axial compression while low n ($n\leqslant 13$) causes lower energy absorption.

Key words: aluminum alloy aging; precipitates; energy absorption; load fluctuation

Cite this article as: ZHANG Long, LI Ke, HE Hong, LI Luo-xing. Influence of prolonged natural aging followed by artificial aging ontensile properties and compressive behavior of a thin-walled6005 aluminum alloy tube [J]. Journal of Central South University, 2021, 28(9): 2647−2659. DOI: https://doi. org/10. 1007/s11771-021-4799-2.

1 Introduction

The 6xxx aluminum alloy extruded structures are widely used for manufacturing both load bearing and energy absorbing members in automobile bodies. The significance to fulfill the safety requirement for passenger has been urging researchers to pay more attention to the crashworthiness and stable energy absorption of these structures [1, 2]. These energy absorbing components are strengthened through aging treatment to obtain high energy absorption efficiency prior to manufacturing the automobile body, cutting, welding, shape forming, for examples. The aging-induced-strengthening processes result from a complex precipitation sequence which is generally accepted as: super-saturated solid solution (SSSS)→GP zones→ $\beta''\rightarrow\beta'\rightarrow\beta$ [3]. The strengthening of the Al-Mg-Si

Foundation item: Project(2019JJ50054) supported by the Natural Science Foundation of Hunan Province, China; Projects(51975201, U1664252) supported by the National Natural Science Foundation of China
Received date: 2020-10-23; **Accepted date:** 2021-01-15
Corresponding author: HE Hong, PhD, Professor; Tel: +86-13787132870; E-mail: hehong_hnu@hnu.edu.cn; ORCID: https://orcid.org/0000-0003-2734-1430

alloys is primarily from the β'' precipitates formed during artificial aging (AA). Before AA, the extruded structures are practically and inevitablly stored at room temperature in factories for several hours to several days due to the storage, transportation and molding, which is identified as natural aging (NA). During NA after solution treatment and quenching, the alloy strength is enhanced due to the formation of Mg/Si clusters [4]. But for the alloys of high solute content (w(Mg)+w(Si)>1%), these formed clusters have a detrimental effect on the formation of β'' precipitation during AA [5]. This is a well-known phenomenon as "negative NA effect" for alloys which are rich in Mg and Si. A general consensus of the explanation for this phenomenon is that it is related with the quenched-in vacancy amount gradually vanishing and the formation of Mg/Si clusters during NA [6, 7], which will both reduce the strength during the thereafter AA. Some researches [8, 9] carried on the precipitation and strengthening mechanisms of these Al-Mg-Si alloys with various NA. They indicated that the existence of Mg/Si clusters in NA reduces the nucleation rate of β'' phase. These clusters are too small to work as nucleation sites for the strengthening precipitates during AA [9] since a greater size than critical one is rather necessary[10]. Subsequently these clusters lead to a lower peak hardness during AA than if the NA could have been shortened [11]. Such negative effect of NA on the subsequent AA hardening depends largely on the chemical composition, machining process and/or aging process. ESMAEILI [12] compared the composition of AA6016 alloy (w(Mg)+w(Si)=1.4%) and AA6111 alloy (w(Mg)+w(Si)=1.5%). They found that AA6016 alloy showed higher yield strength after water-quenching while its hardening rate during NA was much slower than AA6111 alloy. VAUMOUSSE et al [13] compared two different cooling processes resulting in different Mg/Si ratio of AA6111 alloy. They found that Mg/Si ratio was about 0.6 in the as-quenched and about 1.0 in the naturally aged AA6111 alloy. This negative effect of NA also has a great influence on the properties of the extruded structure after extruding and online-quenching process.

When producing aluminum alloy profiles used for vehicle bodies, the extrusion process provides an analogous "solution treatment". In extrusion, the temperature is high enough for the elements to solute and to obtain a high concentration of quenched-in vacancies after water-quenching to room temperature. This process of rapid cooling from a high temperature is requested as the following two reasons: on the one hand, avoid precipitation of coarse non-hardening particles at heterogeneities like dislocations and grain boundaries during rapid cooling; on the other hand, avoid severe diffusion of vacancies to the same type of heterogeneities [14]. Then these extruded profiles are aged during NA followed by AA to gain good mechanical strength and energy absorption ability. EMGLER et al [15] studied the tensile properties and in-plane anisotropy of an age-hardenable AA 6016 aluminum alloy affected by natural aging. It was found that NA enhanced the tensile strength, but had little effect on the anisotropy of the age-hardenable AA 6016. LANGSETH et al [16] found that the deformation mode of an AA 6060 square tube was dependent on tempers. More energy absorption was obtained when the alloy was artificially aged from T4 to T6. HOANG et al [14] made an investigation on the AA6060 alloy with square hollow section artificially aged to three kinds of different tempers (under-aged T6x, peak-aged T6 and over-aged T7) and cooled in water or air. Subquently these aged alloys were subjected to quasi-static axial compression. The results from compressive tests showed that the profile in peak-aged condition after quenching by water exhibits the best energy absorption and fracture was not observed in any kind of the tempered profiles. GRANUM et al [7] investigated the energy absorption capability of a cross-sectional profiles with three different 6xxx alloys (6110, 6061 and 6063 alloy) in accordance with the chemical composition and the thermal-mechanical history (T6, T7 and O). The Mg/Si ratios of 6063, 6061 and 6110 alloys were almost 0.92, 1.45 and 1.15, respectively. The compressive results showed that both of the temper and chemical composition influenced the energy absorption. The profile in the T6 temper absorbed more energy than those in T7 and O tempers. The energy absorption of the profile of 6110-T6 and 6061-T6 seemed to coincide, as well as that with 6110-T7 and 6061-T7, while a notable decline of absorbed energy was obtained in O temper. Whereas the profile with 6063 had strikingly the lowest energy absorption in three different tempers. These studies focus on the

extruded profile of a simple cross-section which is strengthened in a particular temper. But the energy absorption of the extruded profile can be improved by some techniques and aging treatments.

Many studies have been devoted to optimizing the energy absorption capability of Al-Mg-Si alloy tubes by multiple techniques such as determining the tube forming parameters [17, 18] and filling the tube by plastic or metal foams [19, 20]. Other researchers [21] focus on the effect of some particular tempers on the axial compressive behavior of Al-Mg-Si alloy tubes. However, fewer researchers have placed the emphasis on the effect of the variant NA+AA treatments on the axial compressive behavior of thin-walled Al-Mg-Si alloy tubes. In practice, it is efficient and economical to obtain an optimal aging treatment to improve the energy absorption of the extruded tube.

In this paper, a structure of thin-walled 6005 alloy tube is used as energy dissipating parts due to its low weight, easy production and high stiffness. This alloy is specially used for structures of rail vehicles and automobile body mechanisms. After different NA+AA treatments, the compression of tubes varies with the evolution of precipitates, representing different absorption capabilities. The age hardening results in the increase of absorbed energy by promotion of work hardening capability. The objective of this paper is summarized as: 1) to study the precipitate types, density and sizes generated after NA+AA treatments; 2) to study relationship between the precipitate distribution and the mechanical properties; 3) to study the compressive behavior of square thin-walled tubes after NA+AA treatments subjected to axial loading to choose a stable energy absorbed member with fluctuation-less load capacity in consideration of strain hardening exponent.

2 Material and test programs

The material for tensile and compressive tests is a commercial aluminum alloy 6005 with the following chemical composition (in wt%): Si 0.50, Mg 0.56; Fe 0.28; Zn 0.001; Mn 0.02; Cr 0.02; Ti 0.01 and Al balance. The alloy was obtained as billet with Ø85 mm×300 mm. Previous to extrusion, the billets were homogenized at 540 °C for 6 h and extruded as square hollow section profiles with a wall thickness of 2.5 mm and a cross-section of 40 mm×40 mm. The billets were pre-heated to 480 °C before extrusion process. The outlet temperature of the die was 520 − 530 ° C. The extruded profiles were water-quenched online after extrusion. After a short upward time at the start of the extrusion process, the ram speed was kept at constant speed of 7 mm/s. Subsequently, the profile was cut into smaller tubes with a length of 100 mm. Then the samples were stored naturally at room temperature for 1 h to 1 d to 1 week followed by AA at 180 °C for 1 h to 12 h to investigate the influence of the aging condition on the compression performance (for example NA1d+AA1h is remarked as NA1d-1), as shown in Figure 1.

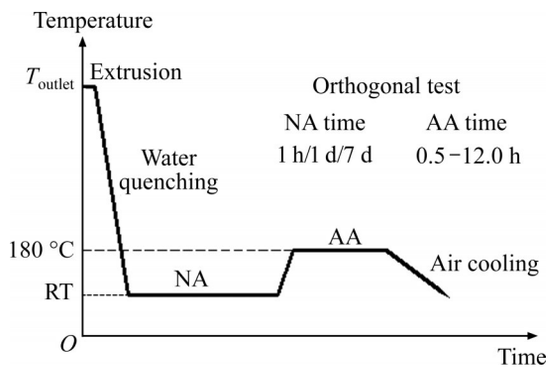

Figure 1 Schemes of NA+AA treatment procedure

Before static tests, the wall thickness of square tube was measured to ensure that the variation in thickness pertinent to the average value was less than 5%. Moreover, the flatness of the sidewalls was also measured with an amplitude less than ±0.03 mm.

The hardness values of aged samples were measured on a Vickers hardness tester with a load of 4.9 N and a dwelling time of 10 s at room temperature. The HV0.5 value along the extruded direction was the average of 10 indentations. Thin foils of 0.4 mm in thickness prepared from the aged samples were mechanically ground to less than 0.015 mm, and then thinned to perforation by twin-jet polishing device using methanol (CH_3OH)-nitric acid solution (volume ratio of 7:3) at −30 to −20 °C and 20 V. The TEM observation of the perforated foils was conducted on a Tecnai G^2 20 TEM operated at a voltage of 200 kV.

The tensile tests were conducted in an Instron 8802 (USA) series universal testing machine with a constant velocity of 2 mm/min. Four test samples were fetched from the sidewalls of an extruded

square tube and parallel to the extrusion direction. The median force level in each aging condition was selected as representative test for calibration of the true stress−strain curves. The compressive tests were conducted with a constant velocity of 5 mm/min, as shown in Figure 2.

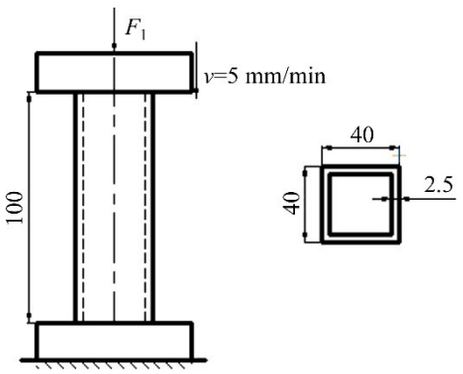

Figure 2 Diagram of compressive test (length unit: mm)

3 Results and discussion

3.1 Hardness and microstructure

Hardness variation of samples during the NA process and after NA+AA treatment is shown in Figure 3. The hardness increases quickly with the increase of NA time within 1000 min. Then the evolution of hardness saturates after around 10000 min (about 1 week) natural aging. The similar phenomenon was observed by CUNIBERTI et al [22] and LI et al [23]. The hardness increases obviously since the samples aged artificially. The shorter the NA followed by AA, the earlier and faster the hardening process started and proceeded. For the sample with the same NA, hardness increases until the AA time prolongs to 6 h, indicating the peak-aged condition. Then peak value persists in a plateau level for several hours (The peak value is $HV_{0.5}$100 for NA1h, $HV_{0.5}$90 for NA1d and $HV_{0.5}$85 for NA1w). The samples with a longer NA followed by AA show slower aging kinetics and decreased apparent hardness. This is the above-mentioned “negative NA effect” for Al-Mg-Si alloy, which is related to the microstructural evolution and many researchers [6, 7, 24, 25] had much interest to investigate it due to its industrial utility. During NA after immediate solution treatment, vacancy-rich Mg/Si clusters have been observed through high resolution transmission electron microscopy (HRTEM) and 3D atom probe [26]. With the prolonged NA, Mg clusters, Si clusters and Mg/Si

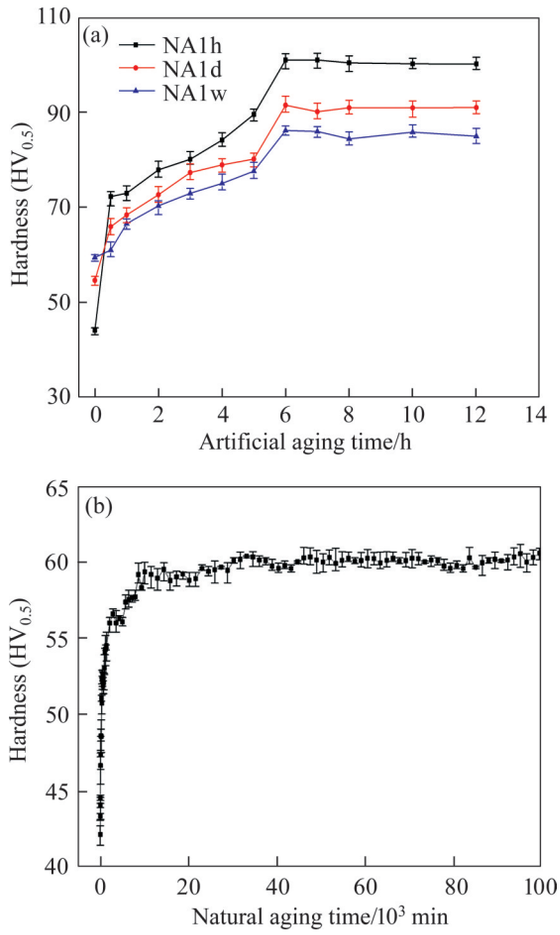

Figure 3 Hardness of aluminum 6005 alloy with NA (a) and NA+AA (b) treatment

co-clusters with atomic ratio of about 1 have been observed [27]. Such clusters are 2−5 nm in size, and cannot be observed by conventional TEM. But the number of atoms in a cluster increases linearly with NA time [28]. With NA proceeding, the clusters are formed by solute atoms and vacancies and the solute is gradually reduced in solid solution. During short AA time (15−30 min), the formation of needle-like β'' precipitates (composition is Mg_5Si_6 [29]) has been well recorded [23]. Then these β'' precipitates grow with AA time and reach their peak value in peak-aged condition when β'' phases are fine and distribute homogeneously. The pronounced hardening after AA 0.5 h in Figure 3 can be attributed to β'' precipitates and the sample in NA1w-0.5 shows the worst effect on hardening.

To investigate the effect of NA on the strengthening precipitates, peak-aged conditions in Figure 3 were selected for transmission electron microscopy (TEM). The TEM images along the $<001>_{matrix}$ zone axis of the peak-aged conditions are

shown in Figure 4. Many fine needle-like precipitates with length of 10 − 40 nm distributed homogeneously in the Al matrix are observed. It has been generally accepted that the β'' precipitates have typical morphologies of needles with size up to 40 Å ×40 Å ×350 Å [30]. Therefore, all of these needle-like precipitates should be designated as β'' precipitates, as shown in Figures 4(a) − (c). For materials with peak-aged condition, with increasing NA time, the number density of and β'' precipitates gets slightly lower, as shown in Table 1. The size of the β'' precipitates grow with increasing NA time. The average length of β'' precipitates in NA1w-6 is 26 nm, about 50% larger than that in NA1h-6, and the number density is 3.5 times lower, resulting in a lower volume fraction. This is believed to be a consequence of local solute and vacancy depletion during the prolonged NA time. The highest number of Mg and Si atoms available to nucleate the hardening precipitates in the case of NA1w-6 may be the reason for the lowest volume fraction of β'' precipitates. The microstructural discrepancy of peak-aged conditions among variant NA times is supported by the tensile tests.

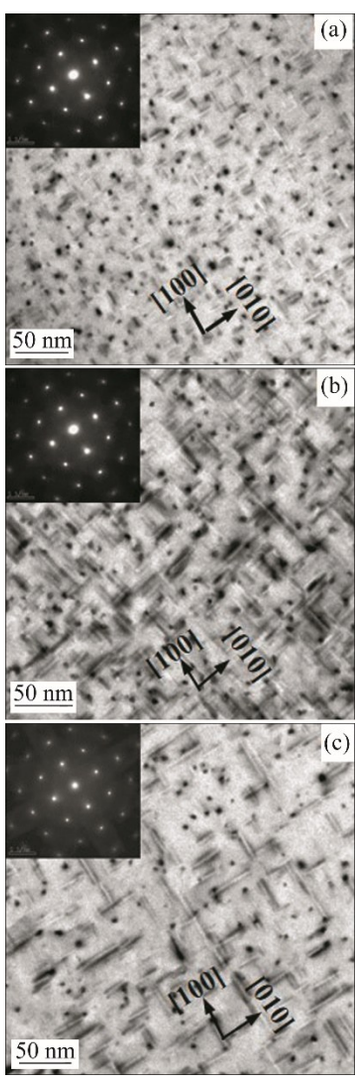

Figure 4 TEM images after different aging treatment: (a) NA1h-6; (b) NA1d-6; (c) NA1w-6

Table 1 Measurements of precipitates in peak-aged conditions

NA+AA treatment	Average length/nm	Average diameter/nm
NA1h-6	12.39	2.78
NA1d-6	19.76	3.04
NA1w-6	26.51	3.12

3.2 Mechanical properties

The tensile tests results are presented in Figure 5, showing the measured yield/ultimate strength (YS/US) and elongation (EL) versus AA time of materials after NA. For samples with the same subsequent AA time, the longer the NA, the lower the YS and US, but the EL reduces little.

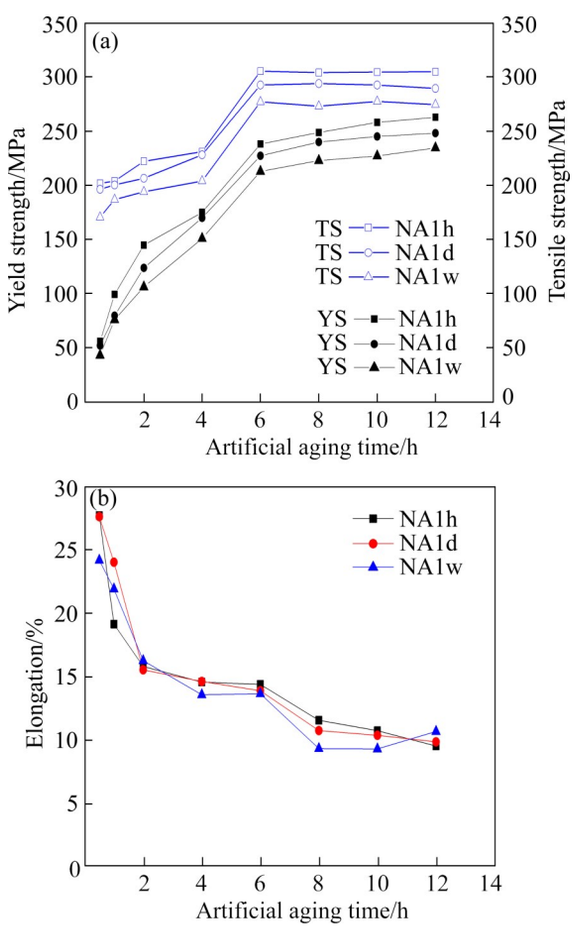

Figure 5 Mechanical properties versus AA time for materials after different NA+AA treatments: (a) Yield and ultimate strength; (b) Elongation

Within the same NA, YS and US increase, and at the same time, the EL decreases obviously with the AA time up to 6 h (which is considered to be the peak-aged condition), afterward US maintains parallel curves while YS increases steadily, as shown in Figure 5(a), but EL drops down inconspicuously in a few hours, as shown in Figure 5(b). In addition, an impressive increase in the YS and US is observed between AA 2h and AA 4h. The strength evolution during NA+AA treatments is closely related to microstructural evolution. It is obvious that peak strength (namely NA 1h+AA 6h, NA 1d+AA 6h and NA 1 week+AA 6h) appears to coincide with the fine distributed homogeneously β'' precipitates and decreases with the increasing size of β'' phase when NA time prolongs from 1 h to 1 week. The weakening in the strengths, under aging conditions, depends on the size, morphology and density of the precipitates. The decrease of strength in peak-aged condition depends on the lower number density of slightly longer and thicker β'' precipitates.

The Ramberg-Osgood equation has been used to describe the nonlinear stress−strain relationships for materials. The strain curves of the equation only feature a plasticity zone. RAMBERG and OSGOOD proposed a simple formula with three parameters (n, σ and ε_p) to describe the stress−strain curve [31]. They thought that the conventional description of metal strain curves by two parameters (elastic modulus and yield point) would be inadequate for efficient design of material outside of Hooke's law. The Ramberg-Osgood model is effective to model the properties of materials and solve the problems of designing structures from plastic materials [31]. In order to illustrate phenomenally the hardening property of the aged materials in this paper, mechanical behavior was supposed to follow Ramberg-Osgood model [32] to fit the true stress−strain curve as:

$$\varepsilon_p = \varepsilon_p + \varepsilon_e = \varepsilon - \frac{\sigma}{E} = 0.002\left(\frac{\sigma}{\sigma_{0.2}}\right)^n \quad (1)$$

where ε_p and ε_e are the plastic strain and elastic strain, respectively; ε is the total true strain; σ is the true stress; E is the elastic modulus; $\sigma_{0.2}$ is the yield stress; n is the strain hardening exponent. The value of n is calculated by the ultimate strength and the corresponding plastic strain.

The relation of strengths and EL and n is represented in Figure 6 and is similar to Figure 5. The parameter n reflects the hardening rate in the plastic process. The larger the n value, the shorter the plastic process in Figure 6(a), and the lower the EL in Figure 6(b). In addition, an extensive increscent in n occurs between AA2h and AA4h. This is related to nucleation and growth of β'' precipitates in Al-Mg-Si alloy. A comparison of the three peak-aged conditions in Figure 4 confirms that the number density of β'' precipitates gets slightly lower, and also the n value gets slightly lower.

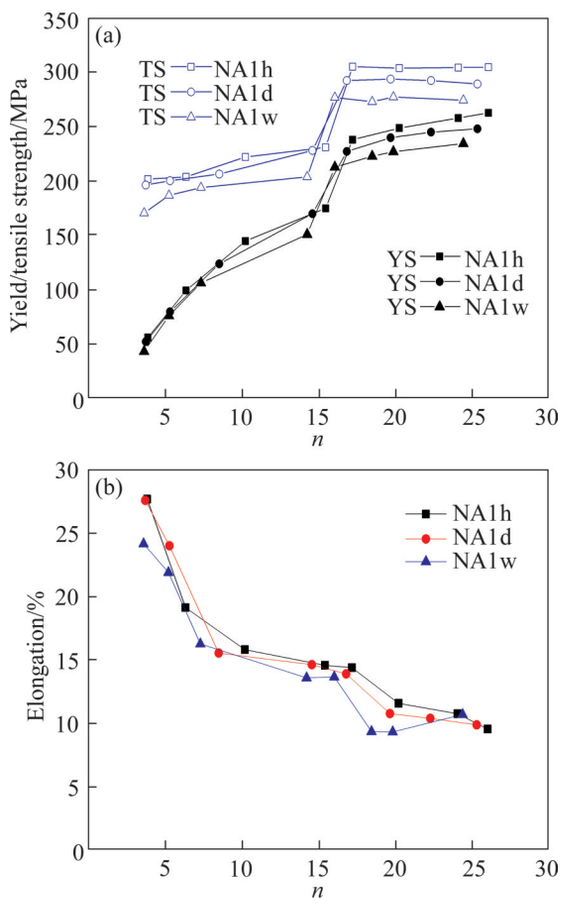

Figure 6 Mechanical properties versus n curves for samples after different NA+AA treatments: (a) Yield and ultimate strength; (b) Elongation

3.3 Compressive behavior

In order to obtain optimum energy absorption in compressive tests, considering the strength and elongation, tubes of moderate yield strength AA1h to AA10h condition after NA in Figure 5 were chosen. The extruded tubes were deformed to 60 mm or overall fracture. The force−displacement curves of tubes after NA+AA treatments are shown in Figure 7, while Figure 8 shows the deformation

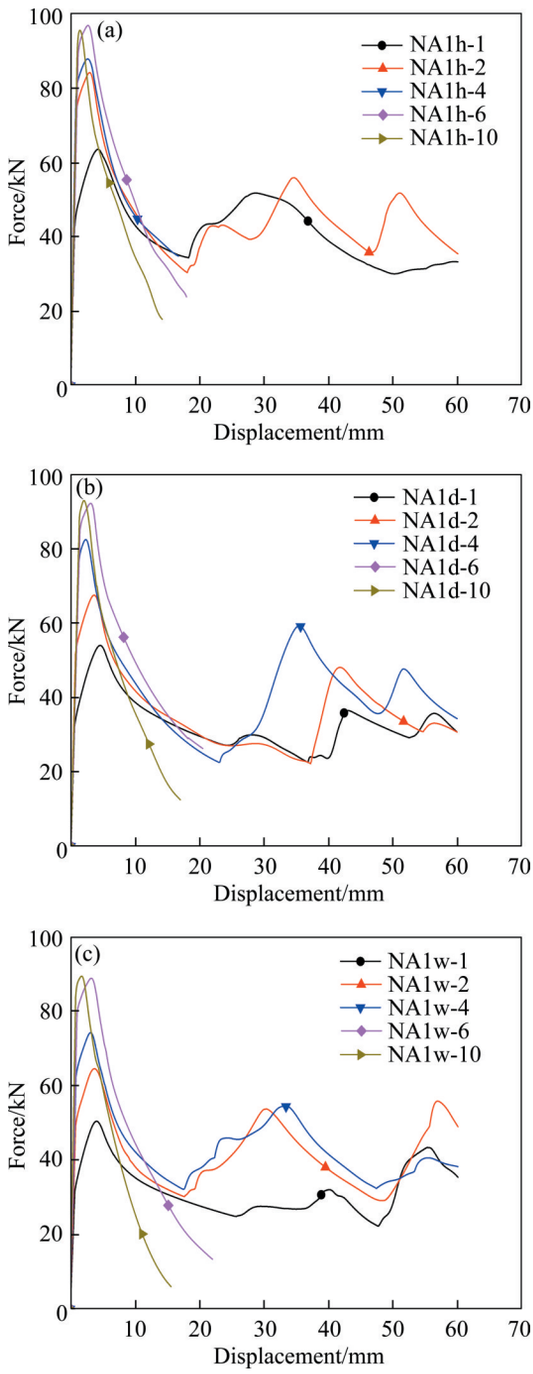

Figure 7 Force – displacement curves from axial compressive tests for samples: (a) NA1h; (b) NA1d; (c) NA1w

patterns and the location of the crack from axial compressive tests. For tubes with the same NA, the longer the AA time, the larger the maximum load (F_{max}). For tubes with the same subsequent AA time, the longer the NA, the lower the F_{max}. An extensive decrease in displacement occurs between AA2h and 4h, which means the deformation of tube from complete folds to crack at the corners. Based on the visual inspection of samples after compressive tests, incipient crack is observed in four corners of tubes in all of conditions with AA upon 4 h. Compared with distinct cracks at the outer corners in NA1h-4 condition, the cracks in tubes emerge at the inner corners of the deformed folds in both NA1d-4 and NA1w-4 conditions, as shown in Figure 8. But the tubes in NA1d-4 and NA1w-4 conditions are still able to absorb energy with growth of small cracks. In comparison, overall fracture of above AA6h tubes occurs during axial compression. The cracks present in peak-aged tubes as well as tubes in NA1h-4 condition when the compression distance is less than 30 mm, as shown in Figures 7(a) – (c), which means large stiffness and incapability to achieve a complete fold.

3.4 Effect of *n* on capacity of energy absorption

The energy absorption of tube is associated directly with the load capacity, compressive capacity and the deformation mode. In the compressive process, the tubes are crushed under the external force to absorb energy. The absorbed energy is represented by the area under the force – displacement curve shown in Figure 7, and thus obtained by integrating as [33]:

$$U = \int_0^{\delta_1} F(\delta)\,\mathrm{d}\delta \tag{2}$$

where F, δ and δ_1 are the instantaneous compressive load, the instantaneous displacement and the compressive length, respectively; U is the absorbed energy. To measure the balance of absorbed energy, the mean compressive load (F_m) is defined as [33]:

$$\left(F_m\right)_{test} = \frac{\int_0^{\delta_1} F(\delta)\,\mathrm{d}\delta}{\delta_1} \tag{3}$$

It should be mentioned that the compressive length is the distance from the origin to the point that the tube bottoms-out or cracks. An ideal U has a constant and fluctuation-less F_m. F_m can be used to characterize the capacity of energy absorption of tube. In particular, for the square Al-Mg-Si alloy tube, the F_m can also be calculated as [16]:

$$\left(F_m\right)_{cal} = 13.06\sigma_0 t^{5/3} b^{1/3} \tag{4}$$

where t=2.5 mm, is the wall thickness of tube; b=B – t, B is the width of tube; σ_0 is the energy equivalent flow stress, which is proposed by LANGSETH et al [16] in consideration of the

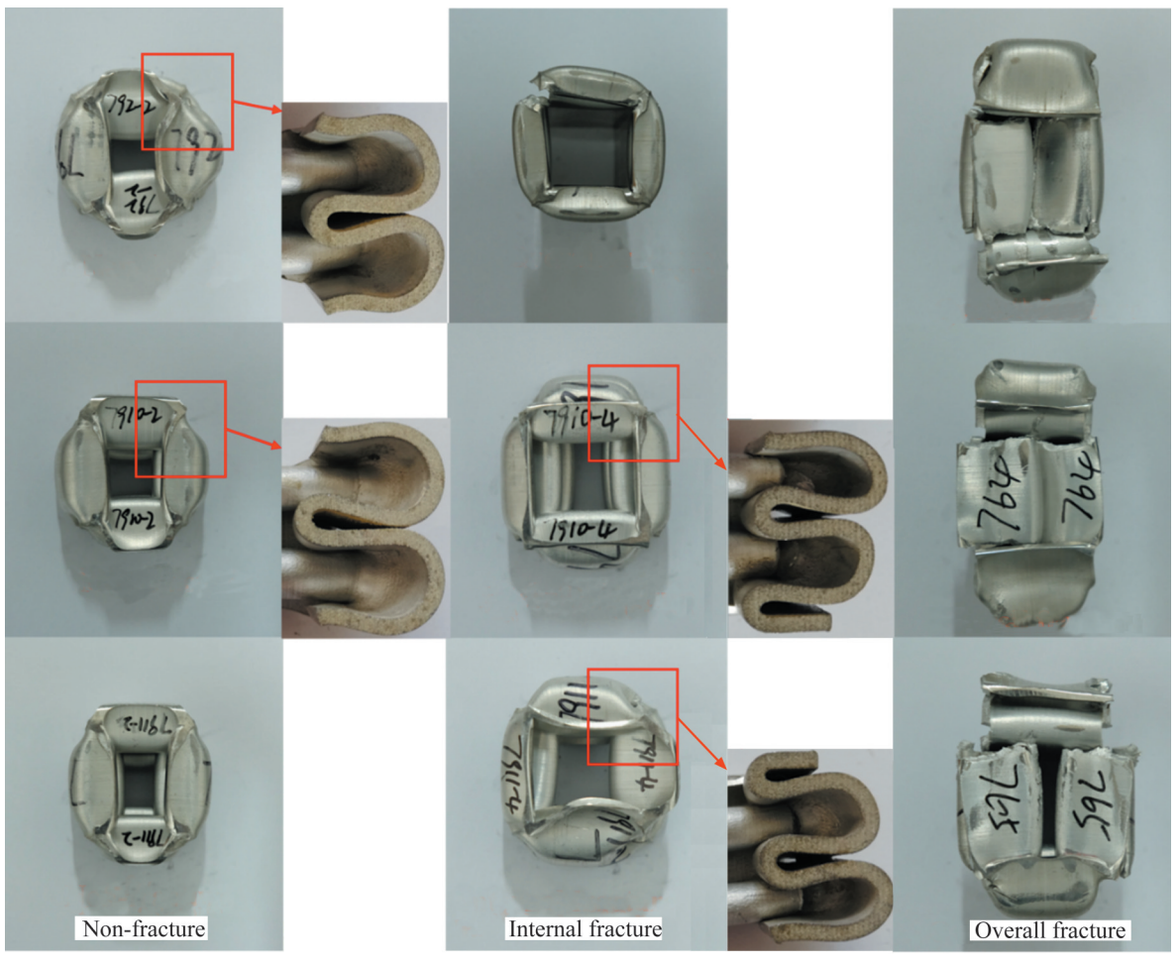

Figure 8 Comparison of deformation patterns of tube in compressive tests after NA+AA treatments

mechanical parameters in Figure 5 which are used as an approximation to the hardening properties.:

$$\sigma_0 = \frac{\sigma_{0.2} + \sigma_u}{2} \tag{5}$$

The relationship between F_m and n of tubes compressed to 60 mm or crack after different NA+AA treatments is shown in Figure 9. The calculated F_m ($(F_m)_{cal}$) vs n is shown in Figure 9(a). The $(F_m)_{cal}$ increases with the increase of n value, namely the theoretical energy absorption increases with the n increasing. In fact, the tested F_m ($(F_m)_{test}$) is varied with n value, as shown in Figure 9(b), due to the structural imperfection or other defects. Excluding the overall fractured tubes, the $(F_m)_{test}$ increases with the increase of n. With the same AA after NA, n decreases with the prolonged NA time, but the $(F_m)_{test}$ decreases from NA1h to NA1d then increases from NA1d to NA1w, which means the energy absorption fluctuates with n increasing when the n value is relatively small (here, n<13). While the $(F_m)_{test}$ of overall-fractured tube decreases with the increase of n when n is large enough (here, n>18), which shows a stable energy absorption. The ratio between $(F_m)_{cal}$ and $(F_m)_{test}$ in Figure 9(c) shows that the calculated data fluctuate along with the experimental data by 1%−25% and in AA6h conditions the fluctuation is within 8%. Furthermore, a much better agreement between the experimental and calculated data ($(F_m)_{cal}/(F_m)_{test}$) is found in the tubes with moderate n value (14<n< 17), which means good energy absorption in these aging conditions.

Under the compressive tests, the structural instability occurs in the local area of tube from the elastic to plastic stage, including the elastic deformation and a small amount of plastic deformation. The 1st derivative of force−displacement at the initial plastic stage shows certain difference after NA+AA treatments due to the multiple startup of the yield stage. The 1st derivative of force−displacement is obtained to depict the plastic stage

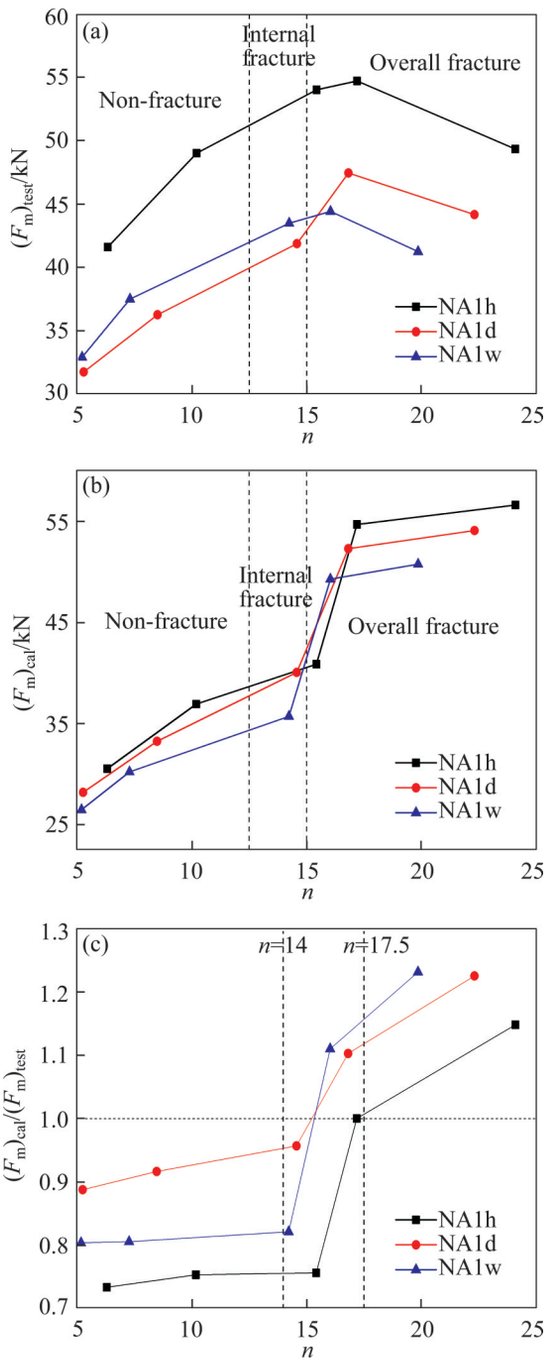

Figure 9 Tested F_m (a), calculated F_m (b), ratio of $(F_m)_{cal}$ to $(F_m)_{test}$ (c)

from the startup of yield stage to F_{max}, as shown in Figure 10. At the start of the plastic stage, the slope of force − displacement plummets, then the descent slows down drastically. For tubes with the same NA, the longer the AA time and the larger the n value, the later the start of the plastic stage, the faster the increase of load to reach F_{max}, the larger the slope of force−displacement except for the peak-aged condition due to the homogeneously distributed β'' precipitates in peak-aged condition, exhibiting excellent plastic performance. Then with the increase of plastic compression, the slope decreases slowly. For tubes with the same subsequent AA, the startup of yield stage in tubes after NA time below 1 d is earlier than the NA time above. The slope for tubes after NA1w prior to AA (Figure 10(c)) shows more steady increase compared to the other two NA conditions (Figures 10(a) and (b)), which means more steady plastic process and stable energy absorption.

The 1st derivative of force − displacement reflects the degree of plastic deformation. A turning point of load emerges when a large 1st derivative drops to small one. By differentiating the 1st derivative of force − displacement curves in Figure 10, the gradient of load slope of the compressive tube can be obtained, as shown in Figure 11. The lowest points in the curves mean the bounce of the structural-load-carrying capacity, namely the critical deformation quantity of instability (D_{cr}). For tubes with the same NA, as shown in Figures 11(a)−(c), the shorter the AA time and the smaller the n value, the faster the structural instability happens when AA time is below 6 h. The range of D_{cr} is from about 0.5 mm to greater than 1 mm. As NA increases, D_{cr} shows fluctuation from NA1h to NA1w, the lowest D_{cr} value appears in NA1d condition when tube is not cracked. The critical load of compressive instability (F_{cr}) can be turned up combining D_{cr} with the force − displacement curves, as shown in Table 2. F_{cr} increases with the increase of n value. This means that with the increase of n value, the capacity of tube to withstand instability is increased.

The ratio of F_m/F_{max} is used to depict the load fluctuation in compressive test. F_m/F_{max} versus n of compressive tubes after different NA+AA treatments is shown in Figure 12. F_m/F_{max} of tubes after NA1h followed by AA fluctuates apparently with the n value. This means that the load fluctuation increases extensively, which is not desired for a good energy absorption member. In comparison, F_m/F_{max} of tubes after NA1d and NA1w decreases with the n value, which means that load capacity shows relatively less-fluctuation. But the non-fracture tubes show fluctuation-more load capacity, and F_m/F_{max} of the cracked tube decreases with the decrease of n value. This means that tube of a large n value (n>15) shows an impressively

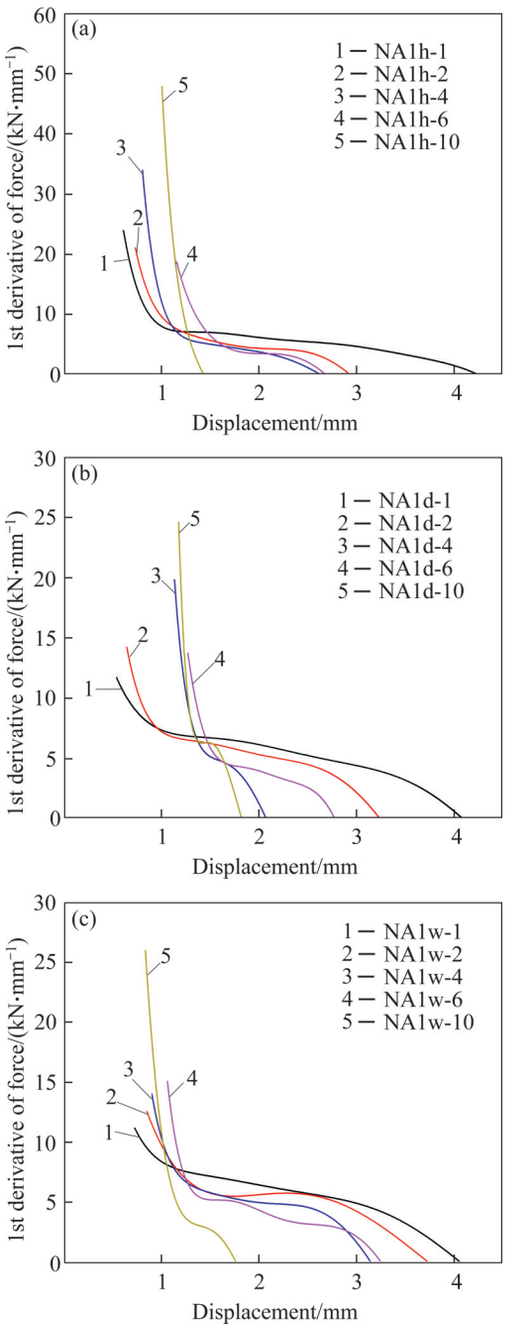

Figure 10 1st derivative of force − displacement curves from startup of yield stage to F_{max} at: (a) NA1h; (b) NA1d; (c) NA1w

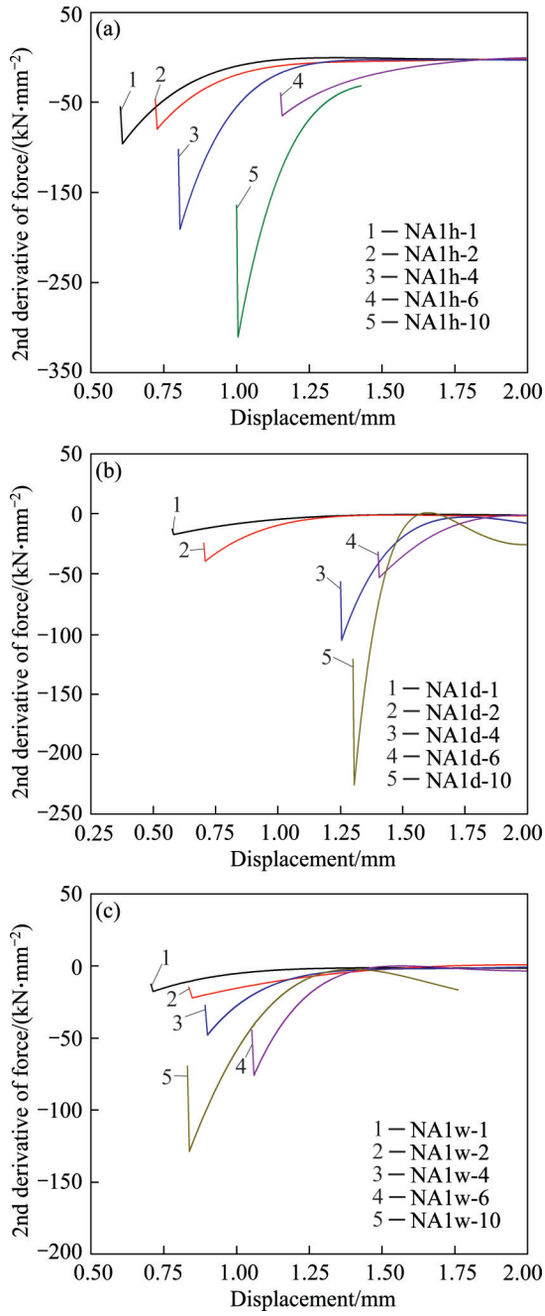

Figure 11 2nd derivative of force−displacement curves of tubes after NA+AA treatments at: (a) NA1h; (b) NA1d; (c) NA1w

fluctuation-less load, which is considered to choose an optimum energy absorbed element. Combined with both of the $n-F_m$ and $n-F_m/F_{max}$ relationship, moderated hardening Al-Mg-Si alloy tube, such as NA1w-4 condition, shows more stable energy absorption and less load fluctuation in this study.

From Figure 4, it is interesting to find that the AA provides the precipitation kinetics to improve the growth of β'' precipitates of 6005 alloy and the nucleation of clusters occurring during the early stages of AA. Then these precipitates are grown along the longitudinal direction. In peak-aged conditions the fine needle-like β'' precipitates distribute homogeneously. The hardening evolution is related with the increasing volume fraction of β'', which is proposed to depict the β'' -dislocation interaction in Al-Mg-Si alloys [8, 34]. The absence of precipitates after NA1w-6 indicates that the Mg/

Table 2 Critical displacement and critical load of tubes after NA+AA treatments

Sample	Parameter	AA1h	AA2h	AA4h	AA6h	AA10h
NA1h	D_{cr}/mm	0.6086	0.7276	0.806	1.157	1.0051
	F_{cr}/kN	42.53	71.32	76.84	89.12	89.31
NA1d	D_{cr}/mm	0.5806	0.7074	1.2549	1.4058	1.3055
	F_{cr}/kN	32.58	51.73	76.5	85.07	88.18
NA1w	D_{cr}/mm	0.7122	0.8468	0.8989	1.0585	0.8368
	F_{cr}/kN	31.58	49.33	62.46	79.39	83.79

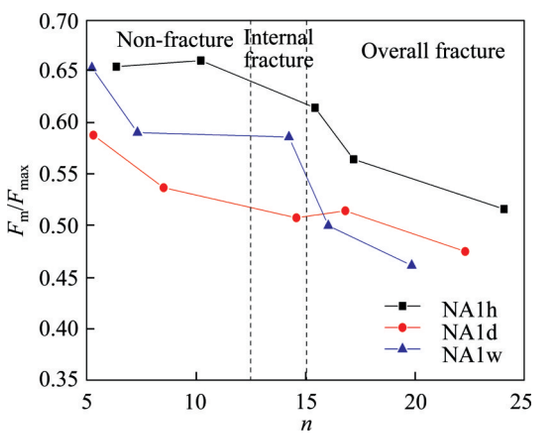

Figure 12 F_m/F_{max} versus n value of compressive tubes after NA+AA treatments

Si clusters formed at NA hinder the formation of β'' precipitates. These results reveal that when solute clusters emerge at NA, the particles for nucleation of β'' precipitates are reduced. Because the solute concentration is lower in the Al matrix, and the precipitates growth is limited by the diffusion field scales with the distance between particles [22]. A lower density in NA results in longer precipitates, which explains the increase of strength with AA time and the slightly lower strength and elongation for NA1w samples compared to NA1h samples.

The strain hardening exponent, n, interprets the relation of the strength and the elongation for the aged sample. The influence of microstructures on strength and elongation can be characterized by n. The growth of β'' precipitates is reflected by the increase of n. In prolonged NA prior to AA, the size and number of density of precipitates are slightly different, which is reflected by the slight difference of n. A comparison of three peak-aged conditions shows that the slightly larger size and lower density of β'' precipitates result in slightly lower n.

The major compressive parameters are the energy absorption capacity and the structural instability. The former reflects the structural-load-carrying capacity and the compressive deformation, and the latter reveals the load fluctuation during compressive. These two parameters are associated directly to the structural imperfection and the stress−strain relationship, which means that the mechanical properties of the material largely influence the structural behavior. The compressive behavior can be properly characterized by n, and further can be determined by the microstructural evolution. The material with low n value causes the tube absorbing low energy and more-fluctuation of load capacity, while the tube with large n value results in crack in four corners. When n is in the moderate value, the material with the homogeneously distributed needle-like β'' precipitates shows good energy absorption and less-fluctuation of load capacity.

4 Conclusions

1) Natural aging induces a negative effect on tensile properties of 6005 aluminum alloy subsequently aged artificially, which is caused by the nucleation and growth of β'' precipitates. This character is represented by the strain hardening exponent n. For samples with the peak-aged condition after increasing NA, the number density of β'' precipitates is lower and the size of β'' precipitates is larger, and the n value is slightly lower, when the NA prolonged from 1 h to 1 week.

2) The relation of the tensile and compressive parameters is established through $n-F_m$ and $n-(F_m/F_{max})$ relationship. The calculated data can well predict the tested data with a moderate n value ($14<n<17$) of the material. Low n ($n<13$) causes lowered absorbed energy, earlier start of structural instability and more-fluctuation of load capacity; while high n ($n>18$) results in the fracture of the extruded tube during axial compression.

3) A better energy absorption, and less load fluctuation with no macroscopic crack during axial compressive can be obtained using moderated n value ($14<n<17$). In this study, tubes after NA1w+AA4h treatment shows a good energy absorption and relative less-fluctuation load in the compressive process.

Contributors

LI Luo-xing provided the concept and edited

the draft of manuscript. HE Hong completed the experiment together and edited the draft of manuscript. ZHANG Long completed the experiment, conducted the literature review and wrote the first draft of the manuscript. LI Ke provided the experimental settings.

Conflict of interest

ZHANG Long, LI Ke, HE Hong and LI Luo-xing declare that they have no conflict of interest.

References

[1] ZHOU Cai-hua, WANG Bo, MA Jia-yao, YOU Zhong. Dynamic axial crushing of origami crash boxes [J]. International Journal of Mechanical Sciences, 2016, 118: 1–12. DOI: 10.1016/j.ijmecsci.2016.09.001.

[2] LIU Zhi-wen, LI Luo-xing, YI Jie, LI Shi-kang, WANG Zhen-hu, WANG Guan. Influence of heat treatment conditions on bending characteristics of 6063 aluminum alloy sheets [J]. Transactions of Nonferrous Metals Society of China, 2017, 27: 1498–1506. DOI: 10.1016/S1003-6326(17)60170-5.

[3] MAISONNETTE D, SUERY M, NELIAS D, CHAUDET P, EPICIER T. Effects of heat treatments on the microstructure and mechanical properties of a 6061 aluminium alloy [J]. Materials Science and Engineering A, 2011, 528: 2718–2724. DOI: 10.1016/j.msea. 2010.12.011.

[4] HIROSAWA S, SATO T. Nano-scale clusters formed in the early stage of phase decomposition of Al-Mg-Si alloys [J]. Materials Science Forum, 2005, 475–479: 357–360. DOI: 10.4028/www.scientific.net/MSF.475-479.357.

[5] YU Wan-yu, HE Hong, ZHANG Wen-kang, LI Luo-xing, SUN Chao-rong. Modulation of the natural aging effect on subsequent artificial aging in Al–Mg–Si aluminum alloys with alloying content ~1 wt% through temperature tuning [J]. Journal of Alloys and Compounds, 2020, 814: 152277. DOI: 10.1016/j.jallcom.2019.152277.

[6] POGATSCHER S, ANTREKOWITSCH R, LEITNER H, EBNER T, UGGOWITZER P J. Mechanisms controlling the artificial aging of Al–Mg–Si alloys [J]. Acta Materialia, 2011, 59: 3352−3363. DOI: 10.1016/j.actamat.2011.02.010.

[7] GRANUM R, MYHR O R, BΦRBIK T, HOPPERSTAD O S. Nanostructure-based finite element analyses of aluminium profiles subjected to quasi-static axial crushing [J]. Thin-Walled Structures, 2018, 131: 769–781. DOI: 10.1016/j.tws.2018.07.034.

[8] ESMAEILI S, LLOYD D J, POOLE W J. Modeling of precipitation hardening for the naturally aged Al-Mg-Si-Cu alloy AA6111 [J]. Acta Materialia, 2003, 51: 3467–3481. DOI: 10.1016/S1359-6454(03)00167-8.

[9] MARIOARA C D, ANDERSEN S J, JANSEN J, ZANDBERGEN H W. The influence of temperature and storage time at RT on nucleation of the β'' phase in a 6082 Al-Mg-Si alloy [J]. Acta Materialia, 2003, 51: 789−796. DOI: 10.1016/S1359-6454(02)00470-6.

[10] POGATSCHER S, ANTREKOWITSCH H, LEITNER H, SOLOGUBENKO A S, UGGOWITZER P J. Influence of the thermal route on the peak-aged microstructures in an Al-Mg-Si aluminum alloy [J]. Scripta Materialia, 2013, 68: 158−161. DOI: 10.1016/j.scriptamat.2012.10.006.

[11] ESMAEILI S, VAUMOUSSE D, ZANDBERGEN M W, POOLE W J, CEREZO A, LLOYD D J. A study on the early-stage decomposition in the Al–Mg–Si–Cu alloy AA6111 by electrical resistivity and three-dimensional atom probe [J]. Philosophical Magazine, 2007, 87: 3797–3816. DOI: 10.1080/14786430701408312.

[12] ESMAEILI S. Effect of composition on clustering reactions in AlMgSi(Cu) alloys [J]. Scripta Materialia, 2004, 50: 155–158. DOI: 10.1016/j.scriptamat.2003.08.030.

[13] VAUMOUSSE D, CEREZO A, WARREN P J, COURT S A. An atom probe study of fine scale structure in AlMgSi(Cu) alloys [J]. Materials Science Forum, 2002, 396–402: 693–698. DOI: 10.4028/www.scientific.net/MSF.396-402.693.

[14] HOANG N H, HOPPERSTAD O S, MYHR O R, MARIOARA C, LANGSETH M. An improved nano-scale material model applied in axial-crushing analyses of square hollow section aluminium profiles [J]. Thin-Walled Structures, 2015, 92: 93–103. DOI: 10.1016/ j. tws.2015.02. 013.

[15] EMGLER O, SCHÄFER C, MYHR O R. Effect of natural ageing and pre-straining on strength and anisotropy in aluminium alloy AA 6016 [J]. Materials Science and Engineering A, 2015, 639: 65–74. DOI: 10.1016/j. msea.2015.04.097.

[16] LANGSETH M, HOPPERSTAD O S, HANSSEN A G. Crash behaviour of thin-walled aluminium members [J]. Thin-Walled Structure, 1998, 32: 127–150. DOI: 10.1016/S02638231(98)00030-5.

[17] ZHANG Xiong, CHENG Geng-dong, ZHANG Hui. Theoretical prediction and numerical simulation of multi-cell square thin-walled structures [J]. Thin-Walled Structures, 2006, 44: 1185−1191. DOI: 10.1016/j.tws.2006.09.002.

[18] SUN Hong-tu, WANG Jian, SHEN Guo-zhe, HU Ping. Energy absorption of aluminum alloy thin-walled tubes under axial impact [J]. Journal of Mechanical Science and Technology, 2016, 30: 3105–3111. DOI: 10.1007/s12206-016-0619-2.

[19] COSTAS M, MORIN D, LANGSETH M, ROMERA L, DIAZ J. Axial crushing of aluminum extrusions filled with PET foam and GFRP: An experimental investigation [J]. Thin-Walled Structures, 2016, 99: 45−57. DOI: 10.1016/j. tws.2015.11.003.

[20] COSTAS M, MORIN D, LANGSETH M, ROMERA L, DIAZ J, ROMERA L. Static crushing of aluminium tubes filled with PET foam and a GFRP skeleton: Numerical modelling and multiobjective optimization [J]. International Journal of Mechanical Sciences, 2017, 131–132: 205–217. DOI: 10.1016/j.ijmecsci.2017.07.004.

[21] FARSHIDI M H. Effect of aging treatment on the crushing behavior of aluminum 6061 alloy tube [J]. Proceedings of the Institution of Mechanical Engineers, Part I: Journal of Materials: Design and Applications, 2014, 229: 389–397. DOI: 10.1177/1464420714524931.

[22] CUNIBERTI A, TOLLEY, RIGLOS M V C, GIOVACHINI G. Influence of natural aging on the precipitation hardening of

an AlMgSi alloy [J]. Materials Science and Engineering A, 2010, 527: 5307−5311. DOI: 10.1016/j.msea.2010.05.003.
[23] LI Hui, LIU Wen-qing. Nanoprecipitates and their strengthening behavior in Al-Mg-Si alloy during the aging process [J]. Metallurgical and Materials Transactions A, 2017, 48: 1990−1998. DOI: 10.1007/s11661-017-3955-7.
[24] MARTINSEN F A, EHLERS F J H, TORSAETER M, HOLMESTAD R. Reversal of the negative natural aging effect in Al-Mg-Si alloys [J]. Acta Materialia, 2012, 60: 6091−6101. DOI: 10.1016/j.actamat.2012.07.047.
[25] TAO G H, LIU C H, CHEN J H, LAI Y X, MA P P, LIU L M. The influence of Mg/Si ratio on the negative natural aging effect in Al-Mg-Si-Cu alloys [J]. Materials Science and Engineering A, 2015, 642: 241 − 248. DOI: 10.1016/j.msea.2015.06.090.
[26] SERIZAWA A, HIROSAWA I, SATO T. 3DAP characterization and thermal stability of nano-scale clusters in Al-Mg-Si alloys [J]. Materials Science Forum, 2006, 519−521: 245 − 250. DOI: 10.4028/www. scientific. net/MSF. 519-521.245.
[27] MURAYAMA M, HONO K, SAGA M, KIKUCHI M. Atom probe studies on the early stages of precipitation in Al-Mg-Si alloys [J]. Materials Science and Engineering A, 1998, 250: 127−132. DOI: 10.1016/S0921-5093(98)00548-6.
[28] ZUROB H S, SEYEDREZAI H. A model for the growth of solute clusters based on vacancy trapping [J]. Scripta Materialia, 2009, 61: 141 − 144. DOI: 10.1016/j. scriptamat. 2009.03.025.
[29] EHLERS F J H, WENNER S, ANDERSEN S J, MARIOARA C D, LEFEBVRE W, BOOTHROYD C B, HOLMESTAD R. Phase stabilization principle and precipitate-host lattice influences for Al-Mg-Si-Cu alloy precipitates [J]. Journal of Materials Science, 2014, 49: 6413−6426. DOI: 10.1007/s10853-014-8371-4.
[30] DADBAKHSH S, KARIMI TAHERI A, SMITH C W. Strengthening study on 6082 Al alloy after combination of aging treatment and ECAP process [J]. Materials Science and Engineering A, 2010, 527: 4758 − 4766. DOI: 10.1016/j.msea.2010.04.017.
[31] MOSTAGHEL N, BYRD R A. Inversion of Ramberg-Osgood equation and description of hysteresis loops [J]. International Journal of Non-linear Mechanics, 2002, 37: 1319−1335. DOI: 10.1016/S0020-7462(02)00025-2.
[32] SHARIFI S, SHAKERI M, FAKHARI H E, BODAGHI M. Experimental investigation of bitubal circular energy absorbers under quasi-static axial load [J]. Thin-Walled Structures, 2015, 89: 42 − 53. DOI: 10.1016/j. tws. 2014. 12.008.
[33] ESMAEILI S, LLOYD D. Modeling of precipitation hardening in pre-aged AlMgSi(Cu) alloys [J]. Acta Materialia, 2005, 53: 5257 − 5271. DOI: 10.1016/j.actamat.2005.08.006.

(Edited by FANG Jing-hua)

中文导读

延长自然时效对6005铝合金薄壁管在人工时效后的拉伸和压缩性能的影响

摘要：本文研究了不同时效处理对6005铝合金薄壁管拉伸和压缩性能的影响。薄壁管样品经过三种不同自然时效后，在180 °C下人工时效0.5−12.0 h，随后进行拉伸和压缩试验。结果表明：在相同自然时效条件下，人工时效时间越长，合金强度越高，同时其伸长率越低，且从塑性变形到开裂的过程越快；而随着自然时效时间的延长，合金在人工时效后的强度降低，但其具有更好的塑性变形能力。由自然时效变化引起的合金强度和塑性的改变，主要是因为随着自然时效时间的延长，主要的强化相β''相的尺寸更大、密度更低。此种特征可由应变硬化指数n进行表征。同时,压缩试验结果表明，当$14<n<17$时，薄壁管的吸能最优；当$n\geqslant 18$时，压缩过程中薄壁管发生开裂；而当$n\leqslant 14$时，薄壁管的吸能较少。

关键词：铝合金时效；二次相；吸能；载荷波动